Static Three-Dimensional Structures Determine Fast Dynamics Between Distal Loci Pairs in Interphase Chromosomes

Guang Shi,[1,*] Sucheol Shin,[1] and D. Thirumalai[1,2,†]

[1] *Department of Chemistry, The University of Texas at Austin, Austin, Texas 78712, USA*

[2] *Department of Physics, The University of Texas at Austin, Austin, Texas 78712, USA*

Abstract

Live cell imaging experiments have shown that, although eukaryotic chromosomes are compact, the distal dynamics between enhancers and promoters are unexpectedly rapid and cannot be explained by standard polymer models. The discordance between the compact static chromatin organization (structure) and the relaxation times (dynamics) is a conundrum that violates the expected structure-function relationship. To resolve the puzzle, we developed a theory to predict chromatin dynamics by first calculating the accurate three-dimensional (3D) structure using static Hi-C contact maps or fixed-cell imaging data. The calculated 3D coordinates are used to accurately forecast the two-point dynamics reported in recent experiments that simultaneously monitor chromatin dynamics and transcription. Strikingly, the theory not only predicts the observed fast enhancer-promoter dynamics but also reveals a novel scaling relationship between two-point relaxation time and genomic separation that is in near quantitative agreement with recent experiments. The theory also predicts that cohesin depletion enhances single-locus diffusion. The acceleration of chromatin loci diffusion upon cohesin depletion are explained in terms of structure-based centrality measure used in graph theory. Our framework shows that chromatin dynamics can be predicted based solely on static experimental data, reinforcing the concept that the three-dimensional structure determines their dynamic behavior. The generality of the theory opens new avenues for exploring chromatin dynamics, especially transcriptional dynamics, across different biological contexts.

* guang.shi.gs@gmail.com

† dave.thirumalai@gmail.com

I. INTRODUCTION

Over the last fifteen years, our understanding of chromatin organization has increased significantly, thanks to advances in experimental techniques, such as Chromosome Conformation Capture and its variants (collectively referred to as Hi-C) [1, 2], as well as multiplexed FISH and other fixed-cell imaging methods [3–10]. These studies, combined with computational modeling [11–19], have revealed the organizational principles that underlie three-dimensional structures of chromosomes at both the ensemble (obtained by averaging over a cell population) and single-cell level. For instance, multiplexed-FISH experiments [8, 9, 20] and polymer theory [21] have been used to show that chromosomes exhibit extensive conformational heterogeneity at the single-cell level, reflecting the dynamical nature of their organization. The combination of experiments and polymer modeling has provided insights into the organization of interphase as well as mitotic chromosomes [22, 23].

Most experimental techniques rely on cell fixation methods, which are fundamentally limiting because they only probe static structures. As a result, our understanding of the potential structure-function relationship, which requires a quantitative understanding of the real-time dynamics of chromatin loci that control gene regulation (transcriptional bursting [24, 25], for example) through enhancer (E)-promoter (P) communications [26], is limited. Recently, live-cell imaging experiments have probed the dynamics of chromatin. Such experiments fall into two categories: (i) Nucleosome positions are tracked without explicitly knowing their genomic identity. This can be used to measure dynamics at the multi-chromosomes and nucleus level [27–30]. (ii) Specific chromatin loci, limited to a small number, are marked and their movement as a function of time are tracked [31]. This can be used to study the dynamics of specific genome regulatory elements, such as CTCF binding and enhancer-promoter interactions [32–35].

In a recent significant development, Brückner et al. [36] employed a three-color labeling scheme to simultaneously probe the dynamics of several pairs of enhancers and promoters along with the transcription of the corresponding gene. The key results of the study, which investigated the one-point and two-point dynamical correlations of chromatin in *Drosophila* cells, may be summarized as follows. (1) On the genomic scale, 58 kb $\leq s \leq$ 3.3 Mb where s is the linear genomic length, chromosomes are compact, resembling the fractal globule (FG) model [37]. This implies that the mean distance, $r(s)$, between two loci should

scale as $r(s) \sim s^{\nu}$ where $\nu = 1/3$ (fractal dimension is $1/\nu$). (2) However, the diffusion exponent, α, characterizing the Mean Square Displacement (MSD) of single chromatin loci and the two-point MSD are both approximately 0.5, which is close to the prediction using the Rouse model [38]. (3) Most notably, the relaxation time (τ), associated with the two-point correlation, scales as a power law, $\tau \sim s^{\gamma}$ where $\gamma \approx 0.7$. Surprisingly, the measured γ value is significantly smaller than the predictions based on both the Rouse model ($\gamma = 2$) and the Fractal Globule (FG) model ($\gamma = 5/3$) [1, 37, 39]. It is striking that the relaxation dynamics between pairs of loci occur on time scales that are significantly faster than predictions using dynamic scaling arguments that are based on the estimates of the mean separation between the loci using the FG or the Rouse model. The apparent lack of connection between the global static structures ($r(s)$ as a function of s) and the observed dynamic behavior requires a theoretical explanation.

Let us briefly explain the origin of the conundrum noted in the experiments [36]. The typical relaxation time, τ_r, of a polymer coil on the scale s (measured along the polymer contour or genomic length) is given by $\tau_r = r^2(s)/D(s)$, where $r(s)$ is the characteristic size of the polymer at scale s, and $D(s)$ is the associated diffusion coefficient. If we assume that $D(s)$ obeys $D(s) \sim s^{-\theta}$ and $r(s) \sim s^{2\nu}$, we obtain the well-known relation $\tau_r \sim s^{2\nu+\theta}$ [40]. On the other hand, the time scale for single monomer diffusion at time τ_r must be consistent with $r(s)$, leading to the relation $\tau_r^{\alpha} \sim r^2(s) \sim s^{2\nu}$. Consequently, the diffusion exponent for a single monomer at intermediate timescales is $\alpha = 2\nu/(2\nu + \theta)$. However, τ_r described above is difficult to quantify directly experiments. Instead, Brückner et al. [36] measured the two-point dynamics using $M_2(t) = \langle ||\boldsymbol{r}_{ij}(t) - \boldsymbol{r}_{ij}(0)||^2 \rangle$ and defined the relaxation time τ as the time at which $M_2(\tau)$ saturates at $\langle r^2(s) \rangle$. The scaling analysis shows that τ follows the same dependence on s as τ_r, namely, $\tau \sim s^{2\nu+\theta}$. This shows that $\gamma = 2\nu + \theta$. The scaling relation,

$$\tau \sim s^{2\nu+\theta} \sim \langle r \rangle^{(2\nu+\theta)/\nu} \tag{1}$$

links the relaxation time, τ, between two loci with the mean spatial distance $\langle r \rangle$ or linear (genomic) distance s. For the Rouse chain, with $\theta = 1$ and $\nu = 1/2$, we find that $\tau \sim s^2$. For FG, with $\theta = 1$ and $\nu = 1/3$, it follows that $\tau \sim s^{5/3}$. The static structures [36] suggests that $\nu = 1/3$, consistent with the FG model. However, the experimentally measured exponent $\gamma \approx 0.7$ deviates from the expected value, $\gamma = 2\nu + \theta = 5/3$. Hence, there is a conundrum.

The failure of the Rouse or FG polymer models to account for the experimental observations [36] prompted us to develop a new theory to explain the fast transcriptional dynamics (relaxation time between pairs of enhancer and promoter). Based on the discordance between global structure and relaxation dynamics one would be tempted to conclude that structure and dynamics are unrelated in chromatin. In this work, we first utilize our previous theory [41] to calculate the three-dimensional (3D) structure of chromosomes using only the measured contact map. Using the ensemble of structures, we investigated the dynamics of distal pairs of chromatin loci. Our model accurately predicts the experimental findings using only the *static* contact map as input, thus resolving the conundrum [36] by demonstrating that the chromatin dynamics can be derived from theory, provided the precise 3D structural ensemble is available. The unexpected scaling behavior observed in the experiment [36] arises from effective long-range interactions among chromatin loci, likely mediated by transcription factors and cohesin. Because our theory is general, it is applicable to various cell types and species, enabling comparative investigations of chromosomal dynamics and mechanics in different species.

II. RESULTS

Outline of the Theory: We developed a theory based on the supposition that knowledge of the static three-dimensional (3D) structure (namely, the knowledge of all the three-dimensional coordinates, $\{\boldsymbol{r}_i\}$ of the chromatin loci) is sufficient to accurately predict the dynamics between arbitrary pairs of loci. The theory is executed in two steps. (i) We first use the measured (Hi-C or related methods) contact map to calculate the precise 3D structures [41] based on the maximum entropy principle, which yields the joint distribution function, $P^{\mathrm{MaxEnt}}(\{\boldsymbol{r}_i\})$. The Hi-C contact map is used to calculate the mean distances ($\langle r_{ij}\rangle$) between loci i and j using polymer physics concepts [8, 42]. The values of $\langle r_{ij}\rangle$ are needed to calculate $P^{\mathrm{MaxEnt}}(\{\boldsymbol{r}_i\})$. The Lagrange multipliers (parameters), k_{ij}, in Eq. 2, ensure that the mean distances between all pairs of loci match the calculated values using $P^{\mathrm{MaxEnt}}(\{\boldsymbol{r}_i\})$. (ii) By interpreting k_{ij} as spring constants in a harmonic potential in the chromatin network, we calculated the dynamical correlation functions using standard procedures used in the theory of polymer dynamics [38]. The details follow.

3D Structures from Hi-C Data: The first step in the theory is the determination of the

ensemble of 3D structures that are quantitatively consistent with the measured contact map. To this end, we used the polymer physics-based HIPPS (Hi-C-Polymer-Physics-Structures) [41] and the related DIMES [43] methods. The HIPPS relates the probability of contact, $\langle p_{ij} \rangle$, between loci i and j, and the mean spatial distance $\langle r_{ij} \rangle$ separating them [8, 42] through the power law relation, $\langle r_{ij} \rangle = \Lambda \langle p_{ij} \rangle^{-1/\alpha}$ with $\alpha \approx 4$. This relation, which was first noted in imaging experiments [8] and subsequently validated in simulations [42], differs from the predictions based on standard polymer models. With $\langle r_{ij} \rangle$ in hand, we formulate the maximum-entropy distribution as a function of the 3D chromatin loci,

$$P^{\mathrm{MaxEnt}}(\{\boldsymbol{r}_i\}) \equiv P^{\mathrm{MaxEnt}}(\boldsymbol{r}_1, \boldsymbol{r}_2, \cdots) = \frac{1}{Z} \exp\left(-\sum_{i<j} k_{ij} ||\boldsymbol{r}_i - \boldsymbol{r}_j||^2 \right), \tag{2}$$

where Z is a normalization constant. The elements, k_{ij}, in Eq. 2 are the Lagrange multipliers which are determined to ensure that the average squared spatial distance between loci i and j matches the target values. We denote the matrix composed of all k_{ij} elements as connectivity matrix, $\boldsymbol{K}$, with $K_{ij} = k_{ij}$ if $i \neq j$ and $K_{ii} = -\sum_{j \neq i} k_{ij}$. The central quantity of interest in our theory is the connectivity matrix, $\boldsymbol{K}$. To determine its elements, k_{ij}, we employed an iterative scaling algorithm designed to match the target $\langle r_{ij} \rangle$ values. The methodology is detailed in prior works [41, 43].

Dynamics from $\boldsymbol{K}$: Although the distribution $P^{\mathrm{MaxEnt}}(\boldsymbol{r}_1, \boldsymbol{r}_2, \cdots)$ (Eq. 2) is calculated using the maximum-entropy principle, we interpret it as a Boltzmann distribution at unit temperature ($k_B T$ is unity) with an effective energy, $H = \sum_{i<j} k_{ij} ||\boldsymbol{r}_i - \boldsymbol{r}_j||^2$. With this identification, k_{ij} may be interpreted as the spring constant between loci i and j. Note that some k_{ij} values are allowed to be negative, which indicates repulsion between chromatin loci. Despite the presence of some negative k_{ij} values, $-\boldsymbol{K}$ is positive semidefinite which ensures that the probability distribution $P^{\mathrm{MaxEnt}}(\boldsymbol{r}_1, \boldsymbol{r}_2, \cdots)$ is well-defined and normalizable. The interpretation that $P^{\mathrm{MaxEnt}}(\{\boldsymbol{r}_i\})$ resembles a Boltzmann distribution allows us to derive the inter-loci dynamics using the framework employed in the context of the Rouse model [38]. Therefore, the eigen-decomposition of the connectivity matrix $\boldsymbol{K}$ may be used to calculate the normal modes. Each independent normal mode obeys the Ornstein-Uhlenbeck process. With this assumption, dynamical quantities such as $M_2(t)$ can be expressed in terms of the eigenvalues and eigenvectors of $\boldsymbol{K}$ (see Supplementary Information for details).

To understand the loci relaxation dynamics, we define the two-point correlation func-

tion $G_2(t)$ as $G_2(t) = \langle r^2(s)\rangle - M_2(t)/2$. The dynamical scaling form of $G(t)$ should be $G_2(t)/G_2(0) \sim g(ts^{-b})$. At $t = \tau$, the curves collapse with $\tau s^{-b} \sim 1$ which leads to $b = 2\nu+\theta$. It has been shown [44] that for $s \ll N$, the scaling form is, $G_2(t) \sim t^{(2\nu-2)/(2\nu+1)}$. $G(t)$ also provides a well-defined way to define the relaxation time τ using $G(\tau) = 1/e$. In our theory, the auto-correlation function for the pair of loci i and j, $G_2^{ij}(t)$, is given by,

$$G_2^{ij}(t) = \langle \boldsymbol{r}_{ij}(t)\boldsymbol{r}_{ij}(0)\rangle = 3\sum_{p=1}^{N-1}(V_{pi} - V_{pj})^2 e^{-t/\tau_p}\big(-\frac{k_BT}{\lambda_p}\big) \tag{3}$$

where p is the normal mode index, and λ_p and matrix $\boldsymbol{V}$ are the eigenvalues and eigenvectors of $\boldsymbol{K}$, respectively. The structure of Eq. 3 matches the Rouse model dynamics [38, 45], except in the chromatin $\boldsymbol{V}$ is non-trivial that requires numerical evaluation using the measured contact maps. The relaxation time for each normal mode is $\tau_p = -\xi/\lambda_p$ where ξ is the friction coefficient. The two-point MSD, $M_2(t)$, is calculated from $G_2(t)$ using $M_2(t) = 2\langle r_{ij}^2\rangle - 2G_2(t)$ where $\langle r_{ij}^2\rangle$ is the square of the equilibrium mean spatial distance between the two chromatin loci. Note that evaluation of Eq. 3 requires only the properties of the matrix, $\boldsymbol{K}$. In the Rouse model $\boldsymbol{K}$ is the polymer connectivity matrix, which is tri-diagonal. In the chromatin problem, it is calculated using Eq. 2 for which the experimental Hi-C or Micro-C contact map is required.

Validating the theory: To validate our theory, let us first show that HIPPS-DIMES (we refer our model as HIPPS-DIMES from now on) correctly recovers the known scaling relations for the Rouse chain, self-avoiding walk (SAW), and FG. The mean spatial distance map for these models can be analytically constructed by using the well-known results, $\langle r_{ij}\rangle = |i-j|^{1/2}$, $\langle r_{ij}\rangle = |i-j|^{3/5}$, and $\langle r_{ij}\rangle = |i-j|^{1/3}$, respectively. Using the analytic expressions for the mean distances, the first step in this theory is to determine $\boldsymbol{K}$ so that target mean pairwise distances $\langle r_{ij}\rangle$ are recovered. In the example, we set the total length of chain to be 1,000, and consider two monomers to be symmetrically located around the midpoint separating them by a linear genomic distance, s. Using $\boldsymbol{K}$, we calculated $G_2(t)$ (Eq. 3) for different models. Fig. 1(a) shows the $G_2(t)$ for an ideal chain for different s values. The relaxation times τ, obtained using $G_2(\tau)/G_2(0) = 1/e$, are shown as solid circles in Fig. 1(b). Similarly, $G_2(t)$ for the SAW and FG are calculated (see Supplementary Figure 3). Fig. 1(b), showing the dependence of τ as a function of s, establishes that the expected scaling of s^2, $s^{5/3}$, and $s^{2.2}$ are correctly reproduced for an ideal chain, the FG, and the self-

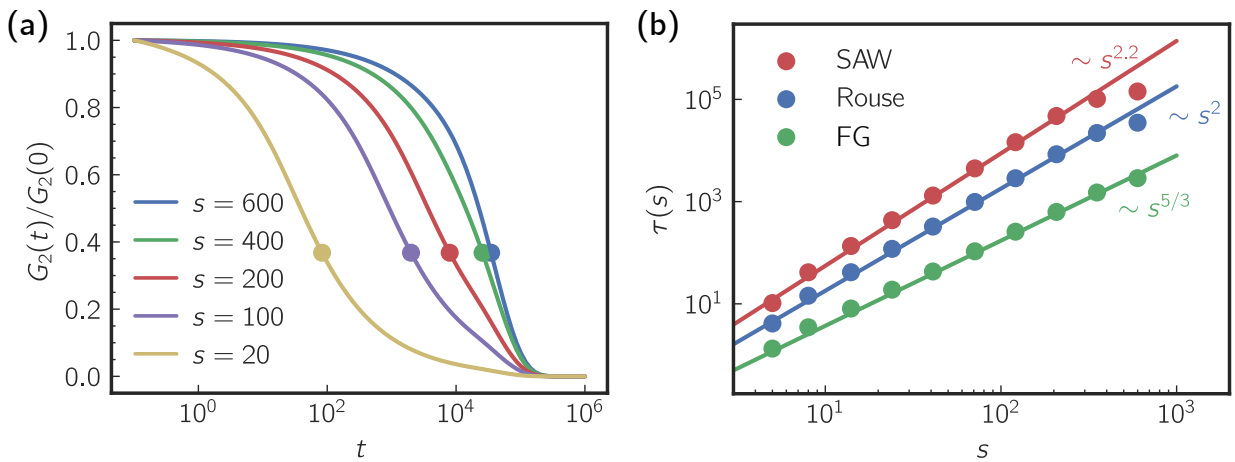

FIG. 1. (a) Normalized two-point relaxation time, $G_2(t)/G_2(0)$, for pair of monomer of indices i and j with $s = |j - i|$. Monomers are selected symmetrically around the center of the chain with $s = |j - i|$ where $i = N/2 - s/2$ and $j = N/2 + s/2$. The results are for the Rouse model with chain length $N = 1,000$. Solid circles indicate the relaxation time τ, defined as $G_2(\tau)/G_2(0) = 1/e$. (b) Relaxation time τ as a function of the sub-chain length s shows $\tau(s) \sim s^x$; $x = 2$ for the Rouse model, $x = 5/3$ for the Fractal Globule (FG), and $x \approx 2.2$ for self-avoiding walk (SAW) chain. The chain length for all three models is $N = 1,000$.

avoiding chain [46], respectively. These calculations show that as long as the 3D polymer structures are known then the relaxation times may be accurately calculated. Needless to say that the dependence of τ with s for homopolymers may be obtained using well-known scaling arguments without resorting to simulations.

To further demonstrate that the theory reproduces the correct dynamical properties, we also tested it against the simulation of self-avoiding polymers in both good and poor solvents. We first performed equilibrium Brownian Dynamics simulations of self-avoiding polymers (see SI for details). We then computed the mean distance matrix from the trajectories. Using the mean distance matrices as input, we calculated the connectivity matrix using the maximum entropy principle (Eq. 2). The connectivity matrix could be used to calculate the single-monomer MSD $M_1(t)$ and two-point MSD $M_2(t)$. Supplementary Figure 4 and Figure 5 show that the theory accurately reproduces the correct dynamics in both good and poor solvents.

Application to experiments: Having established that the theory correctly reproduces

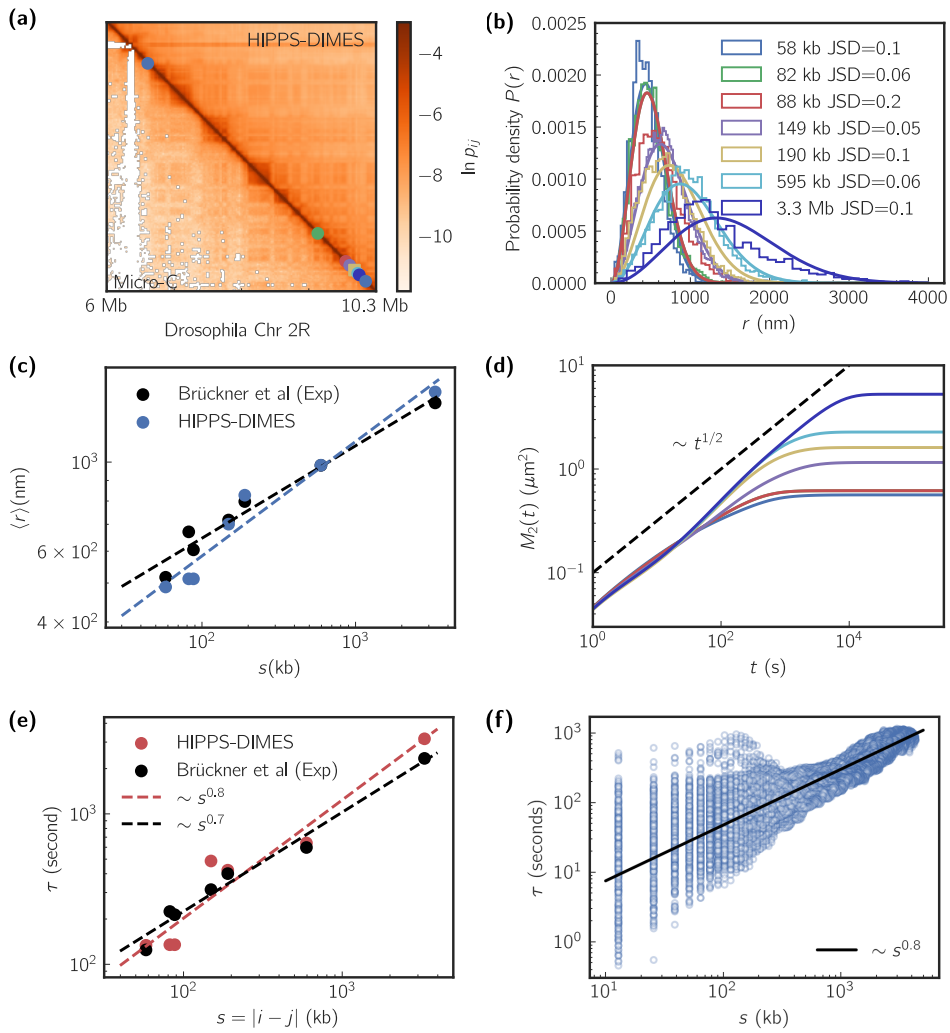

FIG. 2. (a) Comparison between the experimental data (Micro-C) and the predictions using the HIPPS-DIMES method for chromosome 2R in *Drosophila*. The anchor (promoter) and seven different distal loci are represented by squares and circles, respectively. The loci are chosen according to the *eve* promoter-enhancer experimental setup [36]. (b) Distribution of pairwise distances for the seven promoter-enhancer loci pairs. The bar plots show experimental data from [36], while the solid lines represent HIPPS-DIMES predictions. Jensen-Shannon divergence (JSD) between the empirical distributions and model predictions are shown. (c) Comparison of the mean spatial distances $\langle r \rangle$ as a function of the genomic distance s between the experimental measurements and the theoretical predictions. (d) Two-point Mean Square Displacement ($M_2(t)$) calculated from the theory using $M_2(t) = 2\langle r_{ij}^2 \rangle - 2G_2(t)$ with $G_2(t)$ from Eq. 3. (e) Comparison of relaxation times τ as a function of genomic distance s between the experimental observations and theoretical predictions. Black dashed line is our fit to the experimental data. (f). Relaxation time τ versus the genomic distance s (black line is a fit) for all pairs of loci.

the dynamics of an ideal chain, FG as well as self-avoiding chain, we use it to resolve the conundrum that the equilibrium distances between pairs of loci are incompatible with the observed transcriptional dynamics [36]. The derivation leading to Eq. 3 (see SI for details) shows that, if all the loci in the chromatin experience the same friction coefficient ξ, the dynamics based on the HIPPS-DIMES model is fully determined by the connectivity matrix $\boldsymbol{K}$. The expression in Eq. 3 can be numerically computed using the eigenvalues/eigenvectors of $\boldsymbol{K}$ (details are given in the SI). In the HIPPS-DIMES theory, $\boldsymbol{K}$ for any chromosome may be readily calculated from the static contact map (Hi-C or Micro-C) or the imaging data. Since our theory relies on contact map or imaging data to generate the mean distance map, we utilized the published Micro-C data for *Drosophila* embryo cells [47], the cell line used in the experimental study probing the dynamics [36]. Fig. 2(a) compares the HIPPS-DIMES prediction for the contact map with the Micro-C data. In addition to reproducing the contact map faithfully, Fig. 2(b) shows that the distributions, $P(r)$, of spatial distance between promoter and seven enhancers are *quantitatively* recovered (Jensen-Shannon Divergence (JSD) between the empirical distributions and model predictions are calculated and shown). Fig. 2(c) shows the spatial distances, $\langle r \rangle$, as a function of s. These results show that the predictions of the HIPPS-DIMES, using the Micro-C contact map as input, are in excellent agreement with experiments.

Next, we calculated the two-point mean square displacement $M_2(t)$ using Eq. 3 and $M_2(t) = 2\langle r_{ij}^2 \rangle - 2G_2^{ij}(t)$. Use of Eq. 3 requires knowledge of the connectivity matrix $\boldsymbol{K}$, which is the byproduct of the determination of the 3D chromatin coordinates (Eq. 2). Fig. 2(d) shows the time dependence of $M_2(t)$ predicted by our theory for the pairs of E-P distances shown in Fig. 2(b). At long times $M_2(t)$ saturates, approaching the different equilibrium values that depend on the given pair. The rate of approach depends on the specific enhancer and promoter pair.

We then calculated the relaxation time τ. Because the absolute value of the friction coefficient is unknown, we tuned it to achieve the best agreement between the theoretical prediction and experimental value for τ. The fit parameter yields the unit length $l_0 = 147$nm and unit time is $\tau_0 \approx 3.1$s. We used these values to calculate the theoretical predictions for τ versus genomic distance s to compare with experiments. The theoretical prediction for the scaling exponent, γ in $\tau \sim s^\gamma$, is ≈ 0.8 and for experimental data is ≈ 0.7 (Fig. 2(e)). It is important to note that while l_0 and τ_0 are adjustable parameters used to calculate the

absolute values of τ, they do not affect the scaling exponent α. We consider the agreement for τ, and especially γ, between experiment and theory to be striking because the only information that is used in the calculation is the Micro-C static contact map.

Randomly Shuffled Sequence: We then wondered if the introduction of randomness in the Micro-C contact map would lead to a discrepancy between theory and experiment. To this end, we randomly shuffled the pairwise distances in the distance map but retained the first off-diagonal elements. In this way, the polymeric nature of the structure is preserved but the specific WT (wild type) pattern in the Micro-C contact map is destroyed. We then applied HIPPS-DIMES on the shuffled distance map to obtain the connectivity matrix. Comparison of the contact maps between the WT and the randomly shuffled sequence shows (Supplementary Figure 6(a)) that the pattern in the WT contact map is fully disrupted. Supplementary Figure 6(b) shows the mean pairwise distances as the function of the genomic distance. For $s < 10^2$ bps, the mean distance grows roughly as a power law with an exponent of 0.6, demonstrating the polymeric nature is preserved in the random shuffled system. At $s > 10^2$ bps, the mean distances reach the plateau, which is a result of random shuffling. The relaxation time τ for the shuffled sequence is insensitive to the genomic distance (Supplementary Figure 6(c)), which is consistent with the saturation of mean distances. The purpose of this calculation is to show that the scaling of τ as a function of s cannot be captured in random copolymers. The chromatin sequence, reflecting the patterns of activity depicted in histone modifications, and the associated 3D structures should be accounted for precisely.

Loci-dependent relaxation times: Given the remarkable success of our theoretical approach in quantitatively explaining the experimental findings, we calculated all the pairwise relaxation time τ_{ij} where i, j are the loci pair indices. The value of τ_{ij} depends on both i and j, and not merely on the genomic distance $s = |i - j|$ as in the case of homopolymer. On an average, the relaxation time correlates with both s and the mean spatial distance $\langle r_{ij} \rangle$ in non-trivial manner. Fig. 3(a) shows the mean spatial distance map and the relaxation time map, clearly establishing the correlation between the two quantities. Fig. 3(b) shows the scatter plot of $\langle r_{ij} \rangle$ versus τ_{ij}. The results show that, on an average, they are related as $\tau_{ij} \sim \langle r_{ij} \rangle^{2.6}$, which differs substantially from the prediction for the Rouse and the FG models. In particular, the scaling exponent ~ 2.6 is significantly smaller than the Rouse model prediction ($= 4$) and the value for FG ($= 5$).

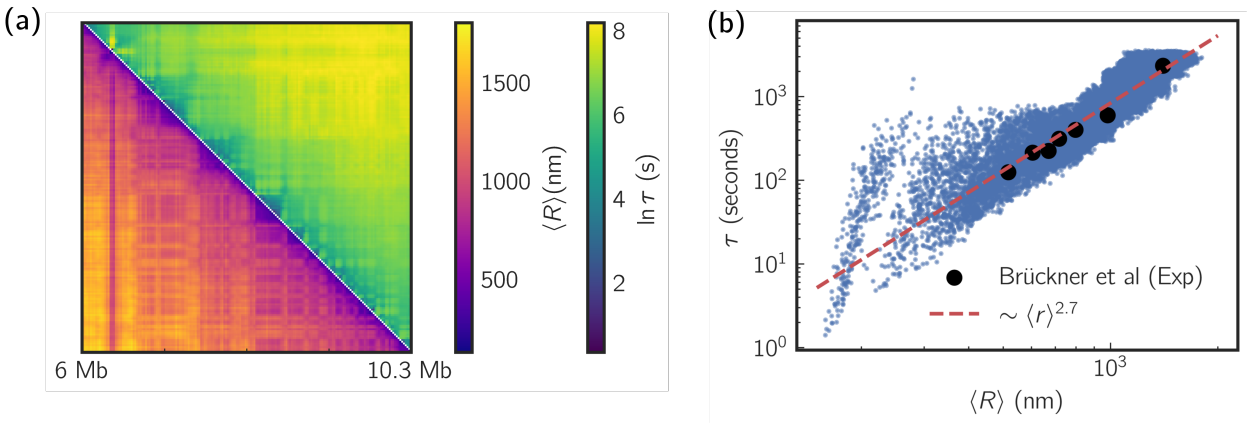

FIG. 3. (a) Comparison between the mean spatial distance matrix (lower triangle) and the map for relaxation time τ (upper triangle). (b) Scatter plot of relaxation time τ versus the corresponding spatial distances $\langle r \rangle$. The black marks are the experimental measurements. The blue markers are the theoretical calculations. The Red dashed line is the fit to the theoretical results.

We then wondered whether the observed scaling can be deduced by considering an effective homopolymer model, in which the mean distance matrix is calculated as the average of the wild-type (WT) distance map over fixed genomic distances. The calculation is intended to assess if a modified scaling relation could be used with the mean distance that is calculated from the contact maps. We computed $r(s)$ by averaging $\langle r_{ij} \rangle$ over $s = |j - i|$, and then applied HIPPS-DIMES to obtain the relaxation time. Supplementary Figure 7 shows the calculated average distance map, demonstrating that $r(s) \sim s^{1/4}$ for $s > 10^2$ kb. Supplementary Figures 7(c) and 7(d) show that the relaxation time scales with genomic distance as $\tau \sim s^{1.1}$ and with mean pairwise distance as $\tau \sim r^4$. Both of these scaling relations are different from the results obtained by considering the full WT contact map. This further demonstrates that arguments in standard polymer physics do not hold for the chromatin, thus underscoring the importance of considering the complete information embedded in the WT contact map. Together, these results show that the relaxation process between a pair of chromatin loci is much faster than predicted by standard polymer models, which provides a structural basis for interpreting the key experimental finding [36]. Importantly, the rapid dynamics between distal loci can be explained by taking into account the actual 3D coordinates of the chromosomes.

Finally, we examined whether promoter-enhancer relaxation is faster than that of non-promoter-enhancer pairs. For this purpose, we computed the distribution of relaxation times

for all loci pairs with the same genomic separation as the corresponding enhancer-promoter pairs. The results, shown in Supplementary Figure 8, reveal distinct trends based on the genomic distance. For very short genomic distances (enhancer-promoter pairs 1 and 2, with separations of 58 kb and 82 kb), the mean relaxation times (133 s and 134 s, respectively) are significantly shorter than the mean relaxation times of all pairs at the same genomic distance (207 s and 240 s). In contrast, for larger genomic distances (all other enhancer-promoter pairs), the mean relaxation times are consistently longer than the corresponding mean values of all pairs with the same separation. These observations suggest that the relaxation dynamics of enhancer-promoter pairs may be influenced by genomic distance in a manner distinct from general locus pairs.

Plausible mechanism for rapid relaxation dynamics in chromatin: To explore the underlying mechanism for the rapid relaxation times between chromatin loci, we calculated the spectrum of eigenvalues, λ_p, associated with, $\boldsymbol{K}$, the connectivity matrix. Interestingly, Fig. 4(a) shows that the scaling of $|\lambda_p|$ with p has a complex structure. There are three distinct regimes in the variation of λ_p with the normal mode p. For $p \leq 10$, we find that $|\lambda_p| \approx p^{1.2}$. In the second regime, $10 \leq p \leq 50$ the eigenvalues increase as $|\lambda_p| \sim p^3$. Finally, $|\lambda_p| \sim p^{1.5}$ for $p \geq 50$. The complicated spectrum for chromatin should be contrasted with the Rouse model for which $|\lambda_p| \sim p^2$ where the inverse of $|\lambda_p|$ maybe interpreted as the relaxation time of N/p segments of the chain. Notably, the decrease in the scaling exponents in the small p regime (Fig. 4(a)) compared to the p^2 scaling of the Rouse model supports the finding that chromatin relaxes more rapidly, consistent with the results for relaxation time τ. In general, for a homopolymer, we expect that $|\lambda_p| \sim p^x$, which implies that the relaxation times scale with respect to the chain length with the same exponent, $\tau_{ee} \sim N^x$. For instance, for the Rouse model, $|\lambda_p| \sim p^2$ and $\tau_{ee} \sim N^2$. If we assume that a similar power law relationship holds between τ_{ee} and p in chromosomes, then expect that $\tau_{ee} \sim N^{1.2}$ if $s \gtrapprox$ 400 kb. To test this prediction, we calculated the end-to-end-distance relaxation times in chromosomes with different lengths. The HIPPS-DIMES-based calculation shows that the end-to-end relaxation time roughly scales linearly with N (Fig. 4(b)) as τ_{ee} varies by over five orders of magnitude. We also computed the eigenvalues for the randomly shuffled system. Supplementary Figure 9(a) shows that $|\lambda_p|$ becomes independent of p for $p \leq 40$, which is is consistent with the findings that τ is insensitive to the genomic distance in the shuffled system. Together, these results suggest that the dynamics of chromosomes are dependent on

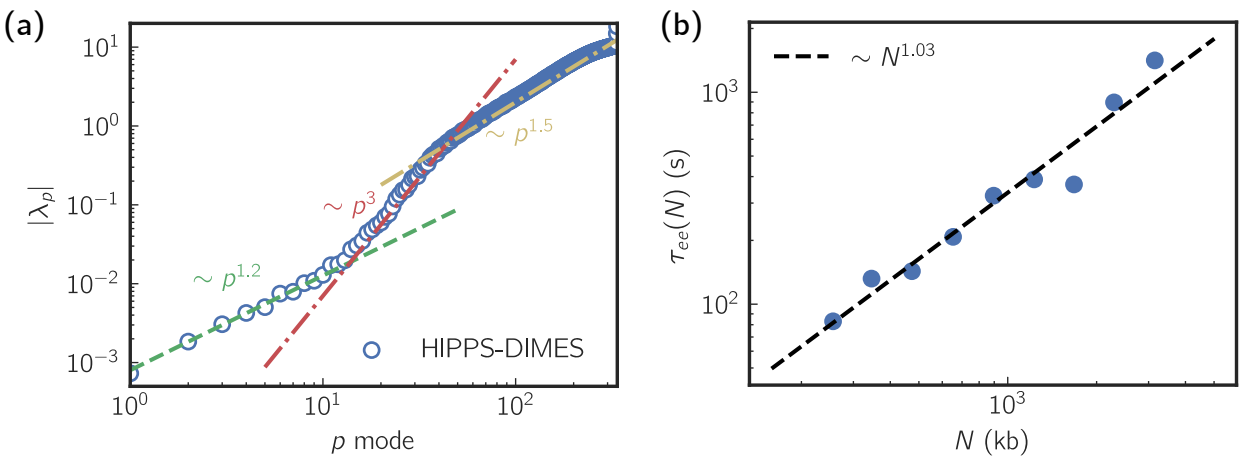

FIG. 4. (a) Scaling of the eigvenvalues, λ_p, of the connectivity matris as a function of p. Three distinct scaling regimes are shown. (b) End-to-end relaxation time τ as a function of chain length N. The dashed line is the fit.

the sequence and the length scale, which is reflected in the observation that the $|\lambda_p|$ exhibits three distinct scaling regimes at different p (different length scales).

First passage time of contact between distal loci: A functionally relevant biophysical property related to the two-point relaxation time is the first passage time of contact between a pair of chromatin loci. A simpler, well-studied, and instructive version of this problem in polymer physics is the cyclization process, which concerns the first passage time for two ends of a polymer chain to meet [46, 48–50]. Let us denote the first passage time of contact as τ_c, which is determined by the search process by which two loci meet. It can be shown that τ_c is directly connected to the two-point relaxation and is governed by the relaxation dynamics between the loci [46, 50], assuming that the threshold for establishing contact is not small. Using a contact threshold of $r_c = 147$nm, we estimated the mean FPT, $\langle \tau_c \rangle$, for all pairs of the chromatin loci. Fig. 5(a) shows that the domain along the diagonal in the τ_c map visually matches the contact domains in the contact map. We then calculated τ_c by averaging over the spatial distance r with fixed genomic distance s. Fig. 5(b) shows that, on an average, the mean τ_c of contact between two chromatin loci scales as $\langle r \rangle^{3.4}$.

We also compared our theoretical predictions with results computed using experimental loci trajectory data. The method for calculating the mean FPT from experimental trajectories is described in the Supplementary Information. As shown in Fig. 5(b), the experimental results (represented by triangle symbols) align closely with our predictions, demonstrating

excellent quantitative agreement between the experiment and the theory.

Interestingly, the calculated scaling exponent of 3.4 is close to 3, which is the theoretical prediction by Szabo, Schulten, and Schulten (SSS) [49] who derived the first passage time of contact under the assumption that single-particle diffusion is governed by dynamics in a potential of mean force, which can be calculated analytically for the Rouse model. The potential of mean force is determined from the distribution of distances between two loci which further leads to [46, 49, 51],

$$\tau_{c,\mathrm{SSS}} = \frac{1}{D}\int_{r_c}^{L} \mathrm{d}x \frac{1}{p(x)}\left(\int_{x}^{L} \mathrm{d}y p(y)\right)^2 \tag{4}$$

where $p(x)$ is the equilibrium distribution of distances x between the two loci with the mean distance $\langle r\rangle$, r_c is the threshold distance distance for contact, and D is the effective diffusion constant. It can be shown using Eq. 4 that $\tau_{c,\mathrm{SSS}} \sim D^{-1} r_c^{-1}\langle r\rangle^3$. This result is consistent with the visual similarity between the contact map and the contact time map shown in Fig. 5(a), as the contact probability scales with the mean distance with an exponent of 3 (in the HIPPS-DIMES model). It is intriguing that the SSS theory, developed for contact formation between a single pair, qualitatively captures the establishment of contacts involving multiple loci pairs. In contrast, the Rouse model does not predict the correct scaling of τ_c as a function of $\langle r\rangle$.

The value of τ_c is important in describing the dynamics of promoter-enhancer communication. If we assume that gene expression is initiated by the formation of contact between promoter and enhancer then the transcription rate can be expressed as $k = 1/(\tau_\mathrm{d}+\tau_c)$, where τ_d is the time required for the downstream processes that ensue after the establishment of contact. By expressing τ_c as a function of the contact probability p_c, with $\tau_c \sim \tau_0 p_c^{-\theta}$, we obtain $\hat{k} = k/k_{\max} = 1/(1 + (\tau_0/\tau_d)p_c^{-\theta})$. This equation is the dynamic analog of the Hill equation with the "cooperativity" parameter θ. Such an equation has been used to model the mean mRNA number as a function of the contact probability between promoter and enhancer [52].

Single-Loci Dynamics and Centrality Measure: Having demonstrated that our theory quantitatively reproduces the experimental data for the two-point dynamics in chromatin loci, we explore the predictions of single-locus dynamics. The single-locus mean square displacement, $M_1(t)$, is computed using Eq. 14 in the Supplementary Information. The prediction for $M_1(t)$ is shown in Fig. 6(a), where each line represents a single chro-

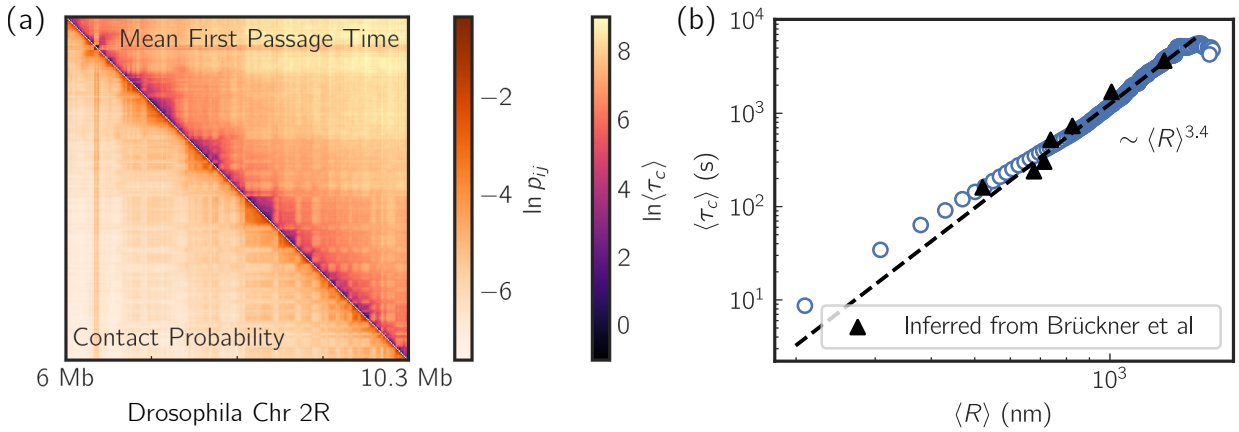

FIG. 5. (a) Comparison between heatmap for the mean first passage time of contact between chromatin loci (upper triangle), $\langle \tau_c \rangle$, and the contact map (lower triangle). The contact is defined with a distance threshold of $r_c = 147$nm. (b) $\langle \tau_c \rangle$ scales as the mean distance $\langle r \rangle$ as a power-law. The dashed line is a guide for the eye. Triangle symbols are the data computed using experimental trajectories data [36].

matin locus. Between the time scale of 1 s $< t < 10^5$ s, $M_1(t)$ scales approximately with an exponent of ~ 0.5, which is close to the prediction of the Rouse model. Next, we calculated the diffusion exponent α and diffusion constant D for each locus by fitting $M_1(t)$ in the time range 1s $< t < 10^5$s using $M_1(t) = Dt^\alpha$. The histogram of α and D reported in Fig. 6(b), yields the ensemble averages of $\langle \alpha \rangle = 0.52$ and $\langle D \rangle = 0.024$ μm^{2}s$^{-1/2}$. The distribution of α is broad as is the spread in the effective diffusion coefficient (Fig. 6(b). Our results show that single-locus diffusion is heterogeneous.

We then investigated the factors that determine the variance in single-locus diffusion. We hypothesize that chromatin loci should generally diffuse more slowly if they have higher local density. Inspired by concepts in graph theory [53], we defined the closeness centrality measure based on the mean pairwise distances. Let us define the centrality of a single locus as C_i, where i is the locus index, as, $C_i = \sum_{j \neq i} r_{ij}^{-m}$, where r_{ij} is the mean pairwise distance between the ith and j^{th} loci, and $m > 0$ is an adjustable parameter. The centrality of a locus is higher when it is in proximity to other loci. Using $m = 3$, we plotted C_i against $M_1(t)$ at $t = 10^2$s (Fig. 6(c)). The results show a negative correlation between the diffusivity of loci and the centrality measure. We recognize that the inverse of the pairwise distance r_{ij} is correlated with the contact probability p_{ij}. We then inspect the correlation

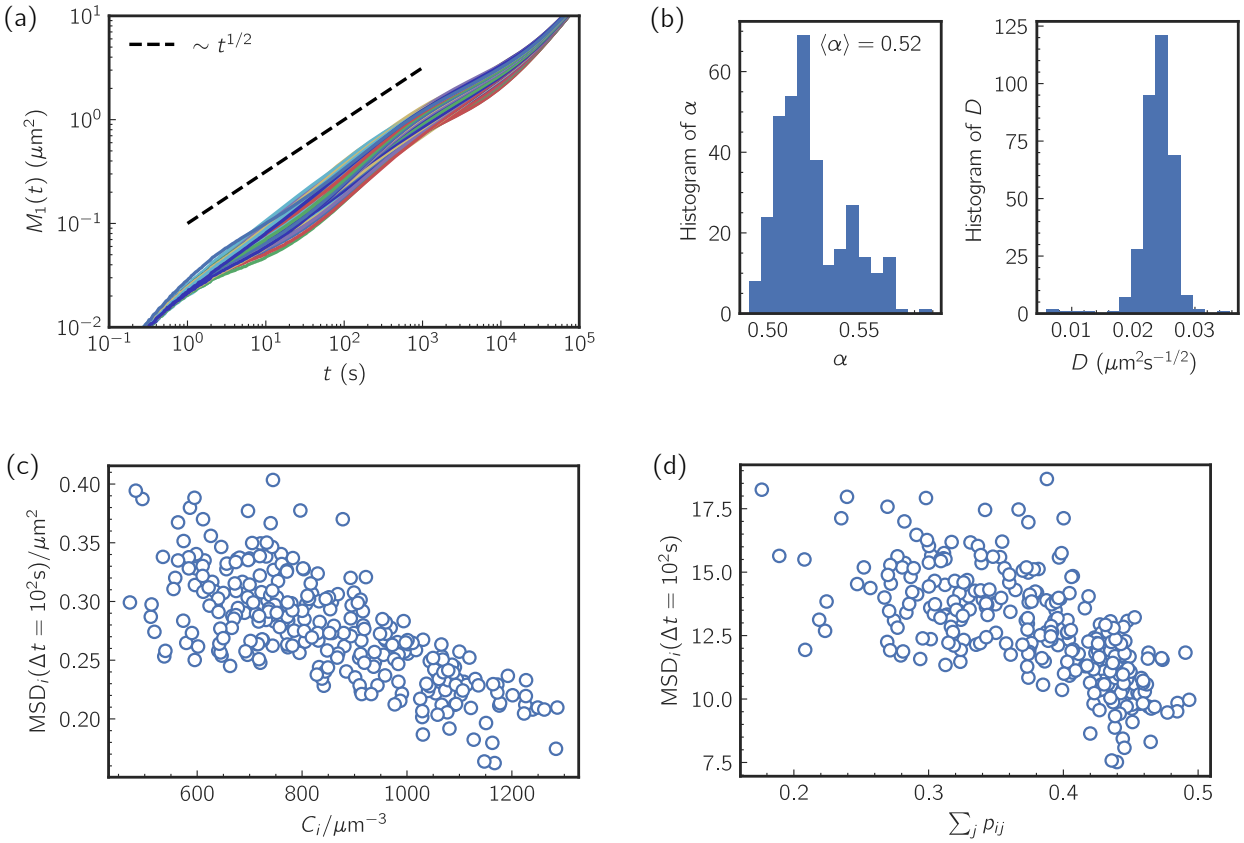

FIG. 6. (a) Single-locus mean square displacement $M_1(t)$. Each curve corresponds to an individual locus. (b) Histogram of the diffusion exponent α and diffusion constant D. (c) Diffusivity, defined as $M_1(t)$ at $t = 10^2$ s, as a function of closeness centrality C_i. (d) Diffusivity $M_1(t = 10^2\text{s})$ as a function of the sum of contact probabilities for each locus i.

between diffusivity $M_1(t = 10^2\text{s})$ and $\sum_{j\neq i} p_{ij}$ and find that these two quantities are indeed anticorrelated (Fig. 6(d)).

Effect of Cohesin Deletion: The generality of our theory allows us to predict the consequences of deleting cohesin on the chromatin loci dynamics. The ATP consuming motor, cohesin, extrudes loops [54, 55] in interphase chromosomes, which results in the formation of Topologically Associating Domains (TADs) revealed in the Hi-C contact map [14, 56]. We took advantage of the imaging data [8] and applied the HIPPS-DIMES method to the experimentally measured mean distance map of human Chromosome 21 for both the wild-type (WT) and cohesin-depleted (ΔRAD21) HCT116 cell lines. After determining the connectivity matrix $\boldsymbol{K}$ by using the measured distance map as constraints, we calculate $M_1(t)$ for each chromatin locus. We then computed the ensemble-averaged mean square

displacement using $\langle M_1(t)\rangle = (1/N)\sum_i M_1^i(t)$, where N is the total number of loci and $M_1^i(t)$ is the mean square displacement for locus i. Fig. 7(a) shows that chromatin loci in cohesin-depleted (ΔRAD21) cells have higher diffusivity (diffusion coefficients) than in the wild-type (WT) cells. The increase in diffusivity ranges between 20% to 40% on the time scales of $10^5 < t < 10^7$. We cannot estimate the absolute value for the time scale because of lack of reference experimental data to benchmark the theory. Therefore, time is reported in reduced units. Since the diffusivity of loci is anticorrelated with their centrality, the results show that cohesin constrains loci dynamics. As a consequence, its deletion leads to increased diffusivity—a prediction that is in quantitative agreement with experiments [34].

We then calculated the relative change in diffusivity as a function of the relative change in centrality. Fig. 7(b) shows that the centrality of chromatin loci decreases after cohesin deletion. Loci exhibiting a greater reduction in centrality typically show a larger percentage increase in diffusivity. Next, we investigate the two-point loci dynamics by calculating the relaxation time τ. Fig. 7(c) shows a heatmap of the relative change in relaxation time between ΔRAD21 and WT cells, $\ln(\tau_{\Delta\mathrm{RAD21}}/\tau_{\mathrm{WT}})$. Fig. 7(c) shows that although chromatin loci dynamics are accelerated after cohesin deletion, the change in two-point relaxation time τ is not uniform but is locus-dependent. For loci located within the TADs, the relaxation time increases after cohesin deletion because the distances between the loci increase. In contrast, loci located at the boundaries of TADs, the relaxation time decreases after cohesin deletion. These predictions are amenable to experimental tests.

We also computed the mode spectrum—characterized by the eigenvalues λ_p—for both wild-type (WT) and cohesin-depleted cells. Supplementary Figure 9(b) shows that the cohesin-depleted system exhibits a distinct gap between the $p = 1$ and $p = 2$ modes, suggesting a separation of relaxation time scales between the entire region and a subset of the region. This gap likely arises from the disruption of two loop extrusion domains present in the WT. Upon cohesin depletion, these domains disappear, and the separation between the $p = 1$ and $p = 2$ modes vanishes. Moreover, we observed a qualitative change in the scaling behavior of $|\lambda_p|$ with respect to p: in WT cells, $|\lambda_p| \propto p^{1.2}$, whereas in the cohesin-depleted cells, $|\lambda_p| \propto p^{1.5}$. The steeper scaling observed in the cohesin-depleted system indicates that small-scale fluctuations dissipate more rapidly, suggesting a loss of coordinated motion across larger chromatin domains.

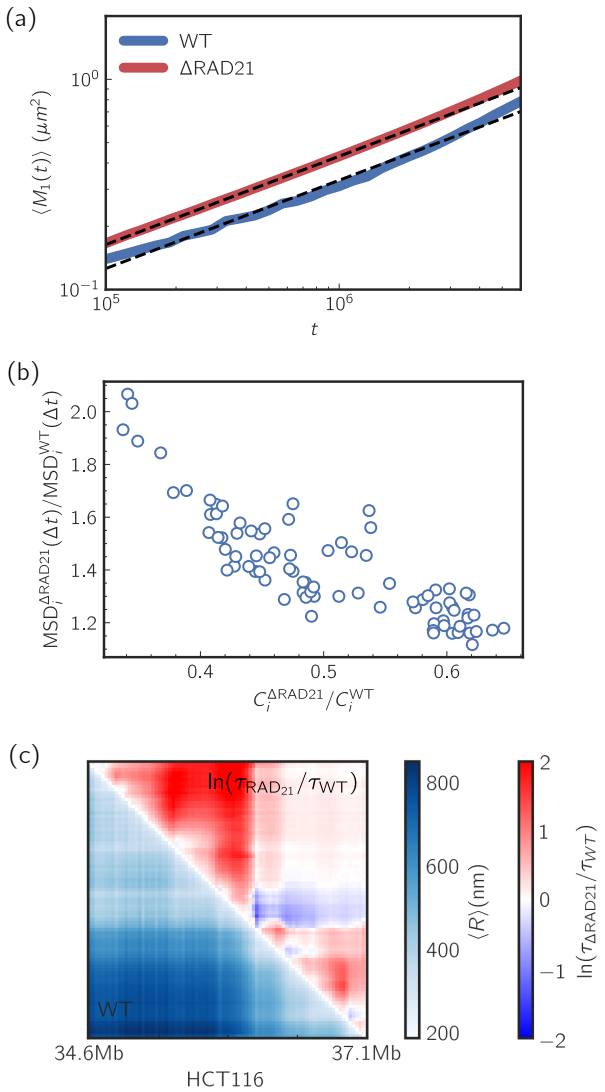

FIG. 7. (a) Ensemble average single-locus mean square displacement $\langle M_1(t)\rangle$ for wild-type (WT) and cohesin-depleted (ΔRAD21) chromosomes. $\langle M_1(t)\rangle$ for each case is calculated by averaging the single-locus $M_1(t)$ over all the chromatin loci. Dashed lines are fits to the data within the time window shown in the figure. (b) Relative change in diffusivity after cohesin deletion vs. relative change in centrality. (c) Lower triangle: mean distance map for WT chromosomes. Upper triangle: relative change in relaxation time after cohesin deletion.

III. CONCLUSION

In this study, we developed a theoretical framework to predict chromatin dynamics from ensemble-averaged static contact maps to make a precise connection between three-

dimensional structure and dynamics. By employing the HIPPS-DIMES methods, we reconstructed the three-dimensional structures of chromatin using the experimental contact maps and derived the connectivity matrix $\boldsymbol{K}$, which encapsulates effective pairwise interactions between chromatin loci. Interpreting this matrix within the context of polymer dynamics allowed us to compute the dynamical correlation functions and predict chromatin dynamics using a generalized Rouse model framework.

Our theory, containing no *adjustable parameter*, accurately reproduces the experimental observations of loci dynamics in *Drosophila* embryo cells, thus resolving the apparent discordance between static chromatin structures and dynamic behaviors highlighted in recent studies [36]. Strikingly, the two-point relaxation times between chromatin loci scale with genomic separation is in excellent agreement with experiments demonstrating that the unexpected rapid relaxation dynamics are a consequence of effective long-range interactions, which could be mediated by factors like transcription factors and cohesin. By analyzing the eigenvalues of the connectivity matrix, we uncovered that the rapid chromatin dynamics exhibit complex, length-scale-dependent behavior, reflecting the hierarchical structural organization of chromosomes. This finding suggests that the dynamics of chromosomes cannot be captured by homopolymer models but requires knowledge of the intricate network of interactions in chromatin. We also used our model to predict the mean first passage times for contact between chromatin loci and found quantitative agreement with results calculated using the experimentally measured loci trajectories [36]. This calculation further supports the notion that chromatin dynamics are intrinsically linked to the precise static three-dimensional structure, which likely play a crucial role in processes such as promoter-enhancer communication.

Additionally, our theory predicts that the heterogeneous single-locus diffusion behavior is dependent on local chromatin density. We found that loci with higher contact probabilities with other loci tend to exhibit slower diffusion, highlighting the influence of the interaction landscape on chromatin mobility. Our exploration of the effects of cohesin deletion revealed that chromatin loci in cohesin-depleted cells exhibit higher diffusivity and the changes in the two-point relaxation times are locus-dependent. This observation underscores the role of cohesin in constraining chromatin dynamics and organizing chromatin structure.

In summary, this work reinforces the concept that the static three-dimensional organization of chromosomes dictates their dynamic behavior, which resolves the conundrum raised

in the experiments [36]. Importantly, we have shown that measurements of the contact map or the distance map using the imaging method are sufficient to calculate the loci-dependent chromatin dynamics. By establishing a direct and quantitative link between chromatin structure and dynamics, our general computational framework opens new avenues for exploring chromatin dynamics in various biological contexts.

CODE AVAILABILITY

The code for the model presented in this work and its detailed user instructions can be accessed at the GitHub repository: https://github.com/anyuzx/HIPPS-DIMES. The data analysis is performed using Python 3.12 in Jupyter Lab. The Python packages used in analyzing data are Scipy, Numpy, and Pandas.

ACKNOWLEDGEMENT

We are grateful to Mauro L. Mugnai for useful comments and discussions. This work was supported by a grant from the National Science Foundation (CHE 2320256) and the Welch Foundation through the Collie-Welch Chair (F-0019).

[1] E. Lieberman-Aiden, N. L. van Berkum, L. Williams, M. Imakaev, T. Ragoczy, A. Telling, I. Amit, B. R. Lajoie, P. J. Sabo, M. O. Dorschner, R. Sandstrom, B. Bernstein, M. A. Bender, M. Groudine, A. Gnirke, J. Stamatoyannopoulos, L. A. Mirny, E. S. Lander, and J. Dekker, Comprehensive mapping of long-range interactions reveals folding principles of the human genome, Science **326**, 289–293 (2009).

[2] S. Rao, M. Huntley, N. Durand, E. Stamenova, I. Bochkov, J. Robinson, A. Sanborn, I. Machol, A. Omer, E. Lander, and E. Aiden, A 3d map of the human genome at kilobase resolution reveals principles of chromatin looping, Cell **159**, 1665–1680 (2014).

[3] J. Fraser, I. Williamson, W. A. Bickmore, and J. Dostie, An overview of genome organization and how we got there: from fish to hi-c, Microbiology and Molecular Biology Reviews **79**, 347 (2015).

[4] F. Bantignies and G. Cavalli, Topological organization of drosophila hox genes using dna fluorescent in situ hybridization, in Hox Genes (Springer New York, 2014) p. 103–120.

[5] B. J. Beliveau, A. N. Boettiger, M. S. Avendaño, R. Jungmann, R. B. McCole, E. F. Joyce, C. Kim-Kiselak, F. Bantignies, C. Y. Fonseka, J. Erceg, M. A. Hannan, H. G. Hoang, D. Colognori, J. T. Lee, W. M. Shih, P. Yin, X. Zhuang, and C.-t. Wu, Single-molecule super-resolution imaging of chromosomes and in situ haplotype visualization using oligopaint fish probes, Nature Communications **6**, 10.1038/ncomms8147 (2015).

[6] S. Wang, J.-H. Su, B. J. Beliveau, B. Bintu, J. R. Moffitt, C.-t. Wu, and X. Zhuang, Spatial organization of chromatin domains and compartments in single chromosomes, Science **353**, 598–602 (2016).

[7] Q. Szabo, D. Jost, J.-M. Chang, D. I. Cattoni, G. L. Papadopoulos, B. Bonev, T. Sexton, J. Gurgo, C. Jacquier, M. Nollmann, F. Bantignies, and G. Cavalli, Tads are 3d structural units of higher-order chromosome organization in drosophila, Science Advances **4**, 10.1126/sciadv.aar8082 (2018).

[8] B. Bintu, L. J. Mateo, J.-H. Su, N. A. Sinnott-Armstrong, M. Parker, S. Kinrot, K. Yamaya, A. N. Boettiger, and X. Zhuang, Super-resolution chromatin tracing reveals domains and cooperative interactions in single cells, Science **362**, eaau1783 (2018).

[9] J.-H. Su, P. Zheng, S. S. Kinrot, B. Bintu, and X. Zhuang, Genome-scale imaging of the 3d organization and transcriptional activity of chromatin, Cell **182**, 1641 (2020).

[10] L. Mirny and J. Dekker, Mechanisms of chromosome folding and nuclear organization: their interplay and open questions, Cold Spring Harbor perspectives in biology **14**, a040147 (2022).

[11] M. Barbieri, M. Chotalia, J. Fraser, L.-M. Lavitas, J. Dostie, A. Pombo, and M. Nicodemi, Complexity of chromatin folding is captured by the strings and binders switch model, Proceedings of the National Academy of Sciences **109**, 16173–16178 (2012).

[12] C. A. Brackley, S. Taylor, A. Papantonis, P. R. Cook, and D. Marenduzzo, Nonspecific bridging-induced attraction drives clustering of dna-binding proteins and genome organization, Proceedings of the National Academy of Sciences **110**, 10.1073/pnas.1302950110 (2013).

[13] D. Jost, P. Carrivain, G. Cavalli, and C. Vaillant, Modeling epigenome folding: formation and dynamics of topologically associated chromatin domains, Nucleic acids research **42**, 9553 (2014).

[14] G. Fudenberg, M. Imakaev, C. Lu, A. Goloborodko, N. Abdennur, and L. Mirny, Formation of chromosomal domains by loop extrusion, Cell Reports **15**, 2038–2049 (2016).

[15] M. Di Pierro, B. Zhang, E. L. Aiden, P. G. Wolynes, and J. N. Onuchic, Transferable model for chromosome architecture, Proceedings of the National Academy of Sciences **113**, 12168–12173 (2016).

[16] G. Shi, L. Liu, C. Hyeon, and D. Thirumalai, Interphase human chromosome exhibits out of equilibrium glassy dynamics, Nature Communications **9**, 10.1038/s41467-018-05606-6 (2018).

[17] L. Liu, G. Shi, D. Thirumalai, and C. Hyeon, Chain organization of human interphase chromosome determines the spatiotemporal dynamics of chromatin loci, PLOS Computational Biology **14**, e1006617 (2018).

[18] M. Di Stefano, J. Paulsen, D. Jost, and M. A. Marti-Renom, 4d nucleome modeling, Current opinion in genetics & development **67**, 25 (2021).

[19] D. Thirumalai, G. Shi, S. Shin, and C. Hyeon, Organization and dynamics of chromosomes, arXiv preprint arXiv:2410.01219 (2024).

[20] E. H. Finn, G. Pegoraro, H. B. Brandão, A.-L. Valton, M. E. Oomen, J. Dekker, L. Mirny, and T. Misteli, Extensive heterogeneity and intrinsic variation in spatial genome organization, Cell **176**, 1502 (2019).

[21] G. Shi and D. Thirumalai, Conformational heterogeneity in human interphase chromosome organization reconciles the fish and hi-c paradox, Nature communications **10**, 3894 (2019).

[22] J. H. Gibcus, K. Samejima, A. Goloborodko, I. Samejima, N. Naumova, J. Nuebler, M. T. Kanemaki, L. Xie, J. R. Paulson, W. C. Earnshaw, L. A. Mirny, and J. Dekker, A pathway for mitotic chromosome formation, Science **359**, 10.1126/science.aao6135 (2018).

[23] A. Dey, G. Shi, R. Takaki, and D. Thirumalai, Structural changes in chromosomes driven by multiple condensin motors during mitosis, Cell Reports **42**, 112348 (2023).

[24] T. Fukaya, B. Lim, and M. Levine, Enhancer control of transcriptional bursting, Cell **166**, 358–368 (2016).

[25] C. Bartman, S. Hsu, C.-S. Hsiung, A. Raj, and G. Blobel, Enhancer regulation of transcriptional bursting parameters revealed by forced chromatin looping, Molecular Cell **62**, 237–247 (2016).

[26] P. Mach and L. Giorgetti, Integrative approaches to study enhancer–promoter communication, Current Opinion in Genetics & Development **80**, 102052 (2023).

[27] A. Zidovska, D. A. Weitz, and T. J. Mitchison, Micron-scale coherence in interphase chromatin dynamics, Proceedings of the National Academy of Sciences **110**, 15555–15560 (2013).

[28] S. S. Ashwin, T. Nozaki, K. Maeshima, and M. Sasai, Organization of fast and slow chromatin revealed by single-nucleosome dynamics, Proceedings of the National Academy of Sciences **116**, 19939–19944 (2019).

[29] R. Barth, K. Bystricky, and H. A. Shaban, Coupling chromatin structure and dynamics by live super-resolution imaging, Science Advances **6**, 10.1126/sciadv.aaz2196 (2020).

[30] K. Wagh, D. A. Stavreva, R. A. M. Jensen, V. Paakinaho, G. Fettweis, R. L. Schiltz, D. Wüstner, S. Mandrup, D. M. Presman, A. Upadhyaya, and G. L. Hager, Dynamic switching of transcriptional regulators between two distinct low-mobility chromatin states, Science Advances **9**, 10.1126/sciadv.ade1122 (2023).

[31] B. Chen, L. Gilbert, B. Cimini, J. Schnitzbauer, W. Zhang, G.-W. Li, J. Park, E. Blackburn, J. Weissman, L. Qi, and B. Huang, Dynamic imaging of genomic loci in living human cells by an optimized crispr/cas system, Cell **155**, 1479–1491 (2013).

[32] H. Chen, M. Levo, L. Barinov, M. Fujioka, J. B. Jaynes, and T. Gregor, Dynamic interplay between enhancer–promoter topology and gene activity, Nature Genetics **50**, 1296–1303 (2018).

[33] J. M. Alexander, J. Guan, B. Li, L. Maliskova, M. Song, Y. Shen, B. Huang, S. Lomvardas, and O. D. Weiner, Live-cell imaging reveals enhancer-dependent sox2 transcription in the absence of enhancer proximity, eLife **8**, 10.7554/elife.41769 (2019).

[34] P. Mach, P. I. Kos, Y. Zhan, J. Cramard, S. Gaudin, J. Tünnermann, E. Marchi, J. Eglinger, J. Zuin, M. Kryzhanovska, S. Smallwood, L. Gelman, G. Roth, E. P. Nora, G. Tiana, and L. Giorgetti, Cohesin and ctcf control the dynamics of chromosome folding, Nature Genetics **54**, 1907–1918 (2022).

[35] M. Gabriele, H. B. Brandão, S. Grosse-Holz, A. Jha, G. M. Dailey, C. Cattoglio, T.-H. S. Hsieh, L. Mirny, C. Zechner, and A. S. Hansen, Dynamics of ctcf- and cohesin-mediated chromatin looping revealed by live-cell imaging, Science **376**, 496–501 (2022).

[36] D. B. Brückner, H. Chen, L. Barinov, B. Zoller, and T. Gregor, Stochastic motion and transcriptional dynamics of pairs of distal dna loci on a compacted chromosome, Science **380**, 1357–1362 (2023).

[37] A. Y. Grosberg, S. Nechaev, and E. Shakhnovich, The role of topological constraints in the kinetics of collapse of macromolecules, Journal de Physique **49**, 2095–2100 (1988).

[38] M. Doi, S. F. Edwards, and S. F. Edwards, The theory of polymer dynamics, Vol. 73 (oxford university press, 1988).

[39] J. D. Halverson, J. Smrek, K. Kremer, and A. Y. Grosberg, From a melt of rings to chromosome territories: the role of topological constraints in genome folding, Reports on Progress in Physics **77**, 022601 (2014).

[40] P. G. De Gennes, Dynamics of entangled polymer solutions. i. the rouse model, Macromolecules **9**, 587–593 (1976).

[41] G. Shi and D. Thirumalai, From hi-c contact map to three-dimensional organization of interphase human chromosomes, Physical Review X **11**, 10.1103/physrevx.11.011051 (2021).

[42] G. Shi, L. Liu, C. Hyeon, and D. Thirumalai, Interphase human chromosome exhibits out of equilibrium glassy dynamics, Nature communications **9**, 1 (2018).

[43] G. Shi and D. Thirumalai, A maximum-entropy model to predict 3d structural ensembles of chromatin from pairwise distances with applications to interphase chromosomes and structural variants, Nature Communications **14**, 10.1038/s41467-023-36412-4 (2023).

[44] K. Polovnikov, M. Gherardi, M. Cosentino-Lagomarsino, and M. Tamm, Fractal folding and medium viscoelasticity contribute jointly to chromosome dynamics, Physical Review Letters

120, 10.1103/physrevlett.120.088101 (2018).

[45] P. E. Rouse et al., A theory of the linear viscoelastic properties of dilute solutions of coiling polymers, The Journal of Chemical Physics **21**, 1272 (1953).

[46] N. M. Toan, G. Morrison, C. Hyeon, and D. Thirumalai, Kinetics of loop formation in polymer chains, The Journal of Physical Chemistry B **112**, 6094–6106 (2008).

[47] E. Ing-Simmons, R. Vaid, X. Y. Bing, M. Levine, M. Mannervik, and J. M. Vaquerizas, Independence of chromatin conformation and gene regulation during drosophila dorsoventral patterning, Nature Genetics **53**, 487–499 (2021).

[48] G. Wilemski and M. Fixman, Diffusion-controlled intrachain reactions of polymers. i theory, The Journal of Chemical Physics **60**, 866–877 (1974).

[49] A. Szabo, K. Schulten, and Z. Schulten, First passage time approach to diffusion controlled reactions, The Journal of Chemical Physics **72**, 4350–4357 (1980).

[50] T. Guérin, O. Bénichou, and R. Voituriez, Non-markovian polymer reaction kinetics, Nature Chemistry **4**, 568–573 (2012).

[51] S. Kwon, H. W. Cho, J. Kim, and B. J. Sung, Fractional viscosity dependence of reaction kinetics in glass-forming liquids, Physical Review Letters **119**, 10.1103/physrevlett.119.087801 (2017).

[52] J. Zuin, G. Roth, Y. Zhan, J. Cramard, J. Redolfi, E. Piskadlo, P. Mach, M. Kryzhanovska, G. Tihanyi, H. Kohler, M. Eder, C. Leemans, B. van Steensel, P. Meister, S. Smallwood, and L. Giorgetti, Nonlinear control of transcription through enhancer–promoter interactions, Nature **604**, 571–577 (2022).

[53] M. E. Newman, Communities, modules and large-scale structure in networks, Nature physics **8**, 25 (2012).

[54] M. Ganji, I. A. Shaltiel, S. Bisht, E. Kim, A. Kalichava, C. H. Haering, and C. Dekker, Real-time imaging of dna loop extrusion by condensin, Science **360**, 102–105 (2018).

[55] C. Dekker, C. H. Haering, J.-M. Peters, and B. D. Rowland, How do molecular motors fold the genome?, Science **382**, 646–648 (2023).

[56] A. L. Sanborn, S. S. P. Rao, S.-C. Huang, N. C. Durand, M. H. Huntley, A. I. Jewett, I. D. Bochkov, D. Chinnappan, A. Cutkosky, J. Li, K. P. Geeting, A. Gnirke, A. Melnikov, D. McKenna, E. K. Stamenova, E. S. Lander, and E. L. Aiden, Chromatin extrusion explains key features of loop and domain formation in wild-type and engineered genomes, Proceedings

of the National Academy of Sciences **112**, 10.1073/pnas.1518552112 (2015).